Revealing the stability and conductivity of 1D structures in 2D semiconducting lattices

Hangbo Zhou,* Viacheslav Sorkin, ZhiGen Yu, and Yong-Wei Zhang*

*Institute of High Performance Computing (IHPC), Agency for Science, Technology and Research (A*STAR), 1 Fusionopolis Way, #16-16 Connexis, Singapore 138632, Republic of Singapore*

E-mail: zhouhb@ihpc.a-star.edu.sg; zhangyw@ihpc.a-star.edu.sg

Abstract

Recent experiments show that one-dimensional (1D) structures in two-dimensional (2D) semiconducting lattices exhibit either metallic or semiconducting behavior, but the underlying mechanisms are unclear. Our theoretical model predicts that couplings between the 1D structures and the 2D lattices via elastic support and electron transfer play crucial roles. The predicted phase diagram shows that elastic support stabilizes the metallic phase when electron transfer is present. Validated by first-principles calculations on MoS_2, we discover two new types of metallic grain boundaries. Our theory provides a robust framework for designing stable 1D metallic structures.

Introduction

The stability of metallic phases in one-dimensional (1D) chains has long been a topic of theoretical interest[1–7] and holds significant potential for applications such as quantum wires[8] and superconductivities[9,10] and topological insulators.[11] However, the Peierls instability theorem

suggests that an isolated metallic 1D structure is generally unstable attribute to charge redistribution.[1] The Su-Shrieffer-Heeger (SSH) model further demonstrates that an equally spaced 1D atomic chain will spontaneously dimerize, resulting in a metal-to-semiconductor (MS) transition regardless of the interatomic bond stiffness.[12,13] Conventional theory, therefore, implies that achieving a stable 1D conducting structure requires overcoming the electronic instabilities.

Recent experimental measurements[14–18] and theoretical investigations[8,19,20] on grain boundaries (GBs) confirm the presence of stable metallic 1D structures, such as the one shown in Figure 1(a). GBs in 2D transition metal dichalcogenides (TMDs) essentially form 1D structures supported by semiconducting 2D lattices. These studies focus on mirror-imaged GBs formed at a 60° misorientation angle within a hexagonal structure. Such GBs are commonly observed in films grown by molecular beam epitaxy[21,22] and chemical vapor deposition[23,24] under chalcogenide-deficient conditions. The observed metallic behavior is explained by charge polarization,[8,19,20,25,26] where discontinuities in the polarization vector are screened by mobile electrons through excitation, leading to metallic behavior. However, this explanation does not account for the stability of the metallic phase.

Conversely, as suggested by Peierls instability, these discontinuities can also be relaxed through formation of charge density waves, leading to lattice distortion or reconstruction. This phenomenon has been observed experimentally,[18,27–30] particularly at low temperatures,[5] and predicted theoretically,[31,32] such as the one shown in Figure 1(b). Constrained by C_{3h} symmetry in the hexagonal 2D lattice, such atomic distortion or reconstruction results in a three-fold increase in the lattice constant,[15,33] as shown schematically in Figure 1. We term this process as trimerization of the GB atoms, which causes a MS transition, thereby challenging the realization of a 1D metallic structure.

A critical issue that remains unresolved is understanding when trimerization occurs or does not occur, as this determines the conductivity of the 1D structure. Previous theory, primarily focused on isolated organic molecular chain[2,3] and quai-one-dimensional lattices,[34,35]

explains instabilities using Fermi-surface nesting and Kohn anomaly to transition temperature. However, these theories do not consider the role of the 2D surroundings. In this study, we address the fundamental question: What are the key factors and criteria for trimerization in a 1D structure within 2D lattices? We propose that electron transfer and elastic support from the 2D lattice play crucial roles in determining stable phases. To verify this hypothesis, we extend the SSH model by connecting a 1D chain with an electron reservoir that allows electron transfer and provides elastic support. Through this model, we analyze the phase diagram of the 1D chain with respect to electron transfer and elastic support. Our results show that the strength of elastic forces acting on the 1D atomic chain significantly influences the its phase once electron transfer is present. Our theory is further supported by first-principles calculations investigating various types of mirror-imaged GBs in MoS_2. Through this practice, we further predict two new types of GBs that exhibit metallic behavior.

Methods

Tight-binding model

We begin by examining a 1D chain without supports using a tight-binding model. Similar to SSH mode, we assume the hopping integral between nearest-neighbor sites, $t_{n+1,n}$, is linearly dependent on their relative displacement: $t_{n+1,n} = t_0 - \alpha(u_{n+1} - u_n)$. We neglect electron spin for simplicity. We analyze trimerization by enforcing periodicity, $u_{i+3} \equiv u_i$, and represent atomic displacements as $u = (u_1, u_2, u_3)$. We find the band structure of the unsupported chain, $\epsilon_{i,k}$, as the roots of the cubic equation:[36]

$$\epsilon_k^3 - (t_{12}^2 + t_{23}^2 + t_{31}^2)\epsilon_k + t_{12}t_{23}t_{31}\cos(3ak) = 0 \tag{1}$$

where a is the untrimerized lattice constant. As shown in Figure 2(a), the band structure of a chain exhibits metallic behavior without trimerization and a bandgap with trimerization.

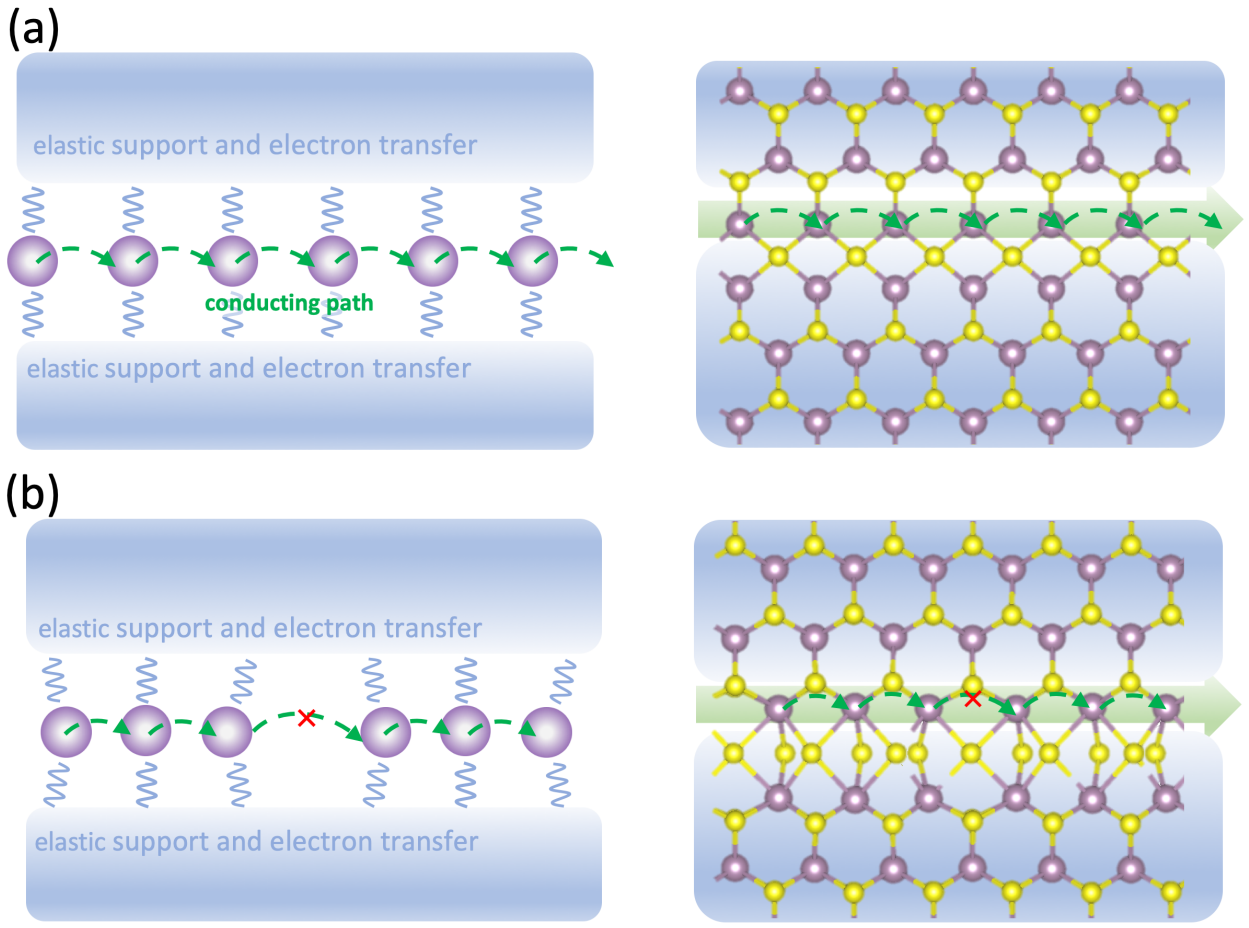

Figure 1: Illustration of (a) untrimerized conducting and (b) trimerized semiconducting one-dimensional structures with two-dimensional supports, inspired by the grain boundaries of 2D MoS_2 shown on the right.

The bandgap is formed at energies of value $\pm t_0$, corresponding to the Fermi level of the chain for one and two conducting electrons, respectively.

Trimerization is energetically favored if it lowers the system's total energy. We evaluate the electronic contribution to the energy, $E_e(u)$, by integrating over the Brillouin zone,

$$E_e(u) = 3a \sum_{i=1}^{m} \int_{-\frac{\pi}{3a}}^{\frac{\pi}{3a}} \frac{dk}{2\pi} \epsilon_{i,k}, \tag{2}$$

where m is the number of conducting electrons. The elastic energy due to trimerization, expressed in terms of the interatomic force constant K, is,

$$E_{ph}(u) = T + \frac{1}{2} K \sum_{n} (u_{n+1} - u_n)^2, \tag{3}$$

where T is the kinetic energy of vibrations. We ignore electron-electron interactions and treat displacements u classically. These assumptions are justified as previous studies show that electron-electron interactions[37–40] and quantum phonon effects[41–43] do not significantly alter the main results concerning spontaneous lattice distortion.

Figure 2(b) illustrates the energy profile of an unsupported chain, showing that the untrimerized state is energetically unfavorable, confirming the Peierls instability which leads to spontaneous trimerization and a MS transition, as seen in Figure 2(c). Trimerization also causes localization of the electronic wavefunction, leading to charge density discontinuities.

Trimerization may be suppressed when the 1D system is supported by a 2D lattice. To model this, we couple the 1D system to an electron reservoir, which allows for electron transfer and provides elastic support:

$$H_e = \sum_{i,k} \epsilon_{i,k} c_{i,k}^\dagger c_{i,k} + \sum_{i,kq} V_{i,kq} (c_{i,k}^\dagger b_q + b_q^\dagger c_{i,k}) + \sum_{q} \epsilon_q b_q^\dagger b_q, \tag{4}$$

where $b_q^\dagger$ and b_q represent creation and annihilation operators for electrons in the reservoir, ϵ_q is the reservoir electron dispersion, and $V_{i,kq}$ determines the coupling strength. The elastic

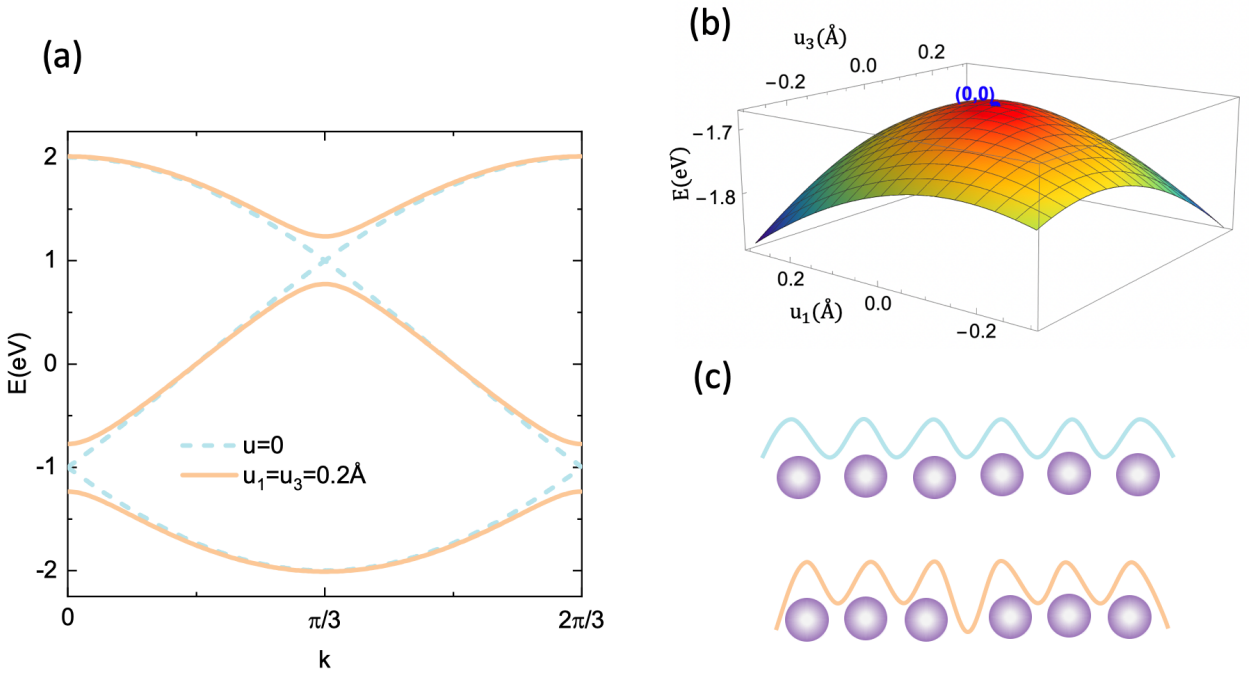

Figure 2: (a) Band structure of unsupported trimerized (solid) and untrimerized (dashed) one-dimensional chains. (b) Energy profile of an unsupported one-dimensional chain versus atomic displacement, with the point (0,0) representing the untrimerized state. u_2 is fixed at 0 as the reference position. (c) Atomic positions of untrimerized and trimerized states with their respective wavefunctions. The parameters are chosen in the order of a typical one dimensional chain $t_0 = 1$ eV, $\alpha = 1.0$ eV/Å, $a = 1.0$ Å.

energy now includes additional restoring forces from the supports:

$$E_{ph}(u) = T + \frac{1}{2}K\sum_{n}(u_{n+1} - u_n)^2 + \frac{1}{2}\sum_{n} K_0 u_n^2, \tag{5}$$

where K_0 represents the strength of the elastic restoring forces.

The evolution of the 1D system with supports involves electron dissipation, described by the quantum master equation:[44,45]

$$\frac{d\rho}{dt} = -\frac{i}{\hbar}[H_S, \rho] + D\rho, \tag{6}$$

where $H_S = \sum_{i,k} \epsilon_{i,k} c_{i,k}^\dagger c_{i,k}$ describes the system's self-evolution, and $D\rho$ represents electron transfer with the supports. We assume that the 2D support is large enough to be an electron reservoir that its electronic states will not be affected by the 1D system. The dynamics of electron transfer can be explicitly described by the Lindblad operator:[46,47]

$$\begin{aligned} D\rho = &\sum_{i,k} \gamma_{i,k}^e (c_{i,k}^\dagger \rho c_{i,k} - \frac{1}{2} c_{i,k} c_{i,k}^\dagger \rho) \\ &+ \sum_{i,k} \gamma_{i,k}^h (c_{i,k} \rho c_{i,k}^\dagger - \frac{1}{2} c_{i,k}^\dagger c_{i,k} \rho) \end{aligned} \tag{7}$$

where the first term describes the transfer of an electron from reservoir to band i while the second term describes the transfer of an electron from band to reservoir, resulting in a hole creation at band i. Their transfer rate $\gamma_{i,k}^{e/h}$ is related to spectra density of the reservoir Γ as $\gamma_{i,k}^e = \frac{1}{2}\Gamma(\epsilon_{i,k}) f(\epsilon_{i,k})$ and $\gamma_{i,k}^h = \frac{1}{2}\Gamma(\epsilon_{i,k})[1 - f(\epsilon_{i,k})]$, where f is the Fermi-Dirac distribution of electrons at the reservoir. The inclusion of a thermal reservoir allowed us to capture temperature effects beyond the limitations of ground-state calculations. This method provides a qualitative understanding of the phase behavior at finite temperatures. In equilibrium, the density function is obtained by solving $d\rho/dt = 0$, which establishes the balance of electron transfer between the system and the reservoir. Thus, the energy of the

system is

$$E(u) = \mathrm{Tr}[\rho_{eq}(H_S - \mu N)] + \frac{1}{2}K\sum_n (u_{n+1} - u_n)^2 + \frac{1}{2}\sum_n K_0 u_n^2 \quad (8)$$

where N is electron number and μ is the reservoir chemical potential, with the energy of the chain as the reference energy, representing the change in free energy once an additional electron is introduced.

First-principles calculation

To verify our theory beyond simplified models, we conducted first-principles calculations on mirror-imaged GBs of MoS_2. To make the lattice periodic in the direction perpendicular to the GB, we calculated two mirror-imaged GBs simultaneously by aligning them in parallel. Convergence tests ensured that the GBs were separated by a sufficient distance (15 Å) to avoid interaction. The band structure of each GB was identified by evaluating its atomic projection at every wavevector for each band. We performed The first-principles density-functional-theory simulations using the Vienna Ab initio Simulation Package (VASP).[48,49] We used the Perdew-Burke-Ernzerhof form of generalized gradient corrections for the exchange and correlation function. Pseudopotentials were derived using projector augmented-wave pseudopotentials with an energy cutoff of 520 eV. To ensure the accuracy of our results, both atomic and unit cell relaxations were performed in all dimensions, with a maximum force criterion of 20 meV/Å. Electronic optimization was achieved with a convergence criterion of 10^{-3} eV. A fine $12 \times 2 \times 1$ Monkhorst-Pack grid was employed to sample the Brillouin zone.

Results and discussion

Results of tight-binding model: Phase diagram

We determine the phase of the 1D structure by evaluating the Hessian matrix, which is defined as $E'' = \frac{\partial^2 E}{\partial u_i \partial u_j}|_{u=0}$. Figure 3(a) shows the smallest element in Hessian versus chemical potential for different elastic force constants K_0 at room temperature. A positive E'' indicates a metallic phase, while a negative E'' indicates a semiconducting phase. The chemical potential of the reservoir determines the number of electrons transferred into the 1D system. When the chemical potential aligns with the Fermi energy of the isolated 1D system ($\mu = -1.0$ eV or $\mu = 1.0$ eV), no electron transfer occurs, and the 1D system transits to a semiconducting phase even with strong elastic forces. However, as the chemical potential moves away from these values, electron transfer occurs, and the elastic force constant K_0 plays a crucial role in suppressing the trimerization. To clearly illustrate these effects, we project the chemical potential regions of semiconductor phase to the bottom of the figure. We can observe that the semiconductor region quickly narrows down with increasing elastic force constants. This implies that electron transfer required for the 1D system to remain metallic decreases significantly with increasing elastic force constants.

The phase diagram at various temperatures is shown in Figure 3(b-d). At all temperatures, the semiconducting region narrows with increasing K_0 , eventually disappearing above a critical elastic force. At low temperatures, two peaks in the phase diagram indicate the Peierls instability, predicting a MS transition in the unsupported 1D system. As temperature increases, these peaks diminish, smearing the ground states around the Fermi level of the 1D system and mitigating the Peierls instability. This phenomenon indicates a temperature dependent phase transition which has been observed.[5] Figure 3(d) presents the phase diagram under the extreme condition of 3000 K, investigated for theoretical interest to assess the GBs' response to thermal excitation. The results indicate that, at this high temperature, the metal-semiconductor transition is suppressed, leading to an expanded region of the

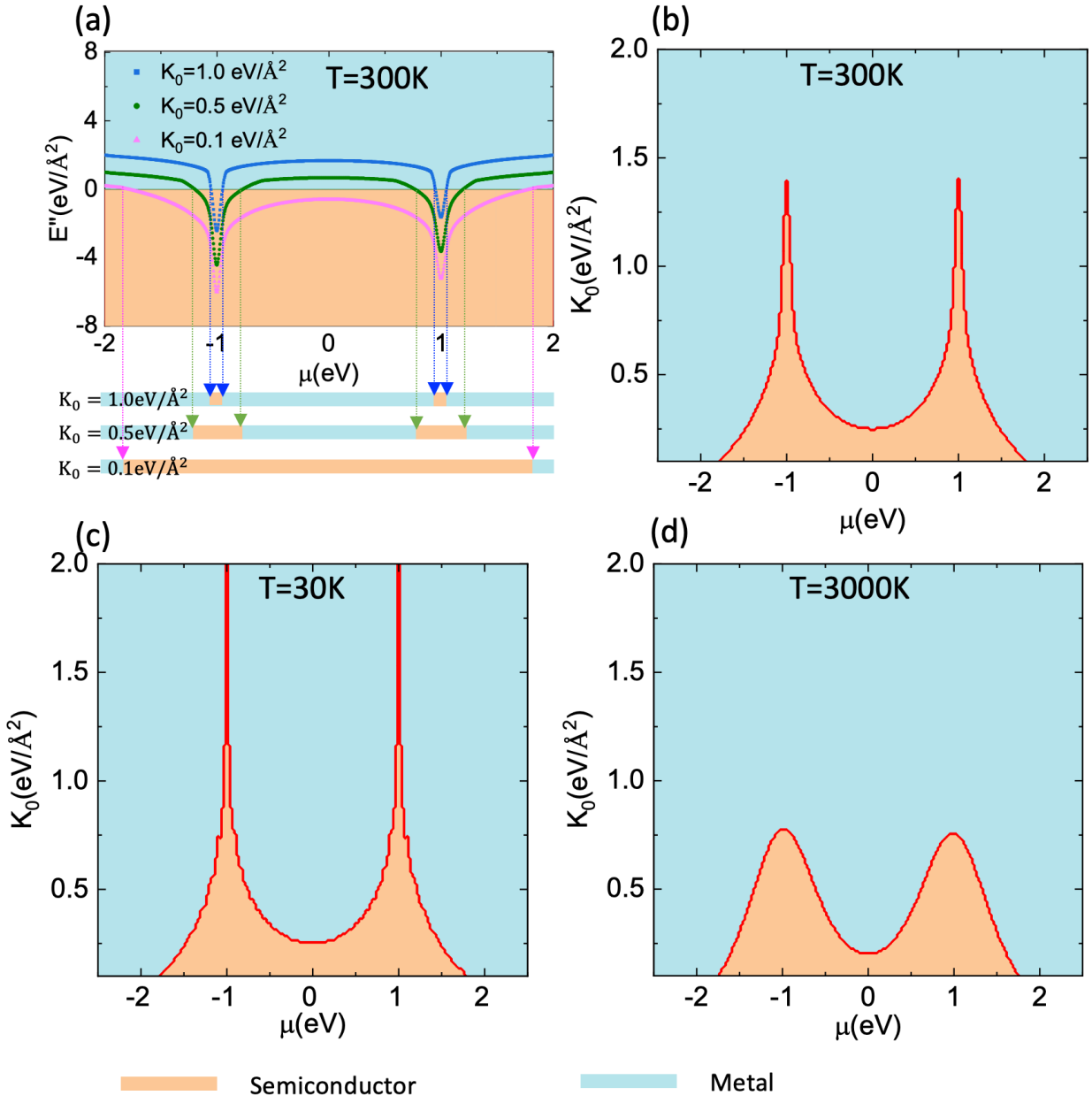

Figure 3: (a) Energy Hessian at different elastic force constants K_0 and chemical potential μ. (b-d) Phase diagram of conductivity in phase space of elastic constant K_0 and chemical potential μ, across different temperatures. The parameters are $t_0 = 1$ eV, $\alpha = 1.0$ eV/Å, $a = 1.0$, and $K = K_0$. White band approximation is used for the reservoir spectra density.

metallic phase.

Results from first-principles calculation

Semi-conducting grain boundaries

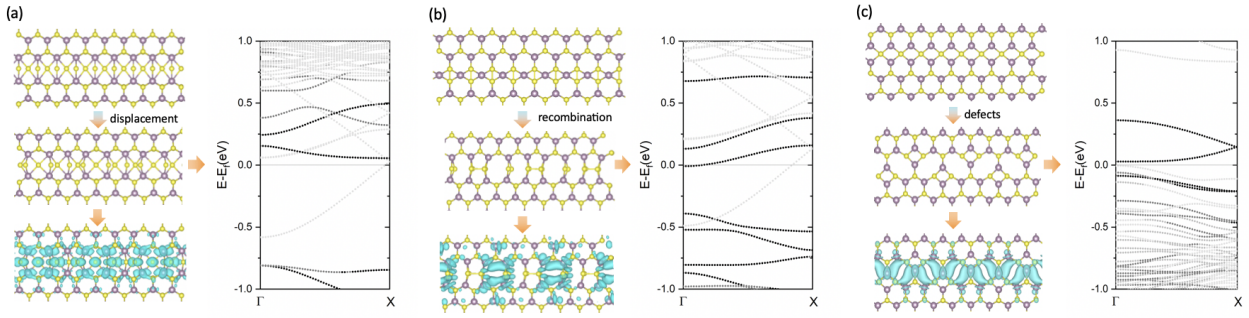

Figure 4: MoS_2 grain boundaries that undergo metal-to-semiconductor transition include (a) S-linked mirror-imaged grain boundaries, (b) Mo-linked mirror-imaged grain boundaries, and (c) mirror-imaged grain boundaries with periodic defects. For each type, the pre-relaxation structure, fully relaxed structure, square of the electron wavefunction, and band structure are shown in order. The isosurface level of the electron density plot is 0.258e/Å^3. The gray scale in the bandstructure indicates the weights of projection on the grain boundary atoms.

First, we explored GBs that undergo a metal-semiconductor transition due to trimerization, as shown in Figure 4. The low formation energies of the GBs (see Figure S1 in the Supporting Information) are consistent with previous calculations,[50–53] and indicate their thermodynamic stability. The stability of these GBs at finite temperatures is further verified through ab initio molecular dynamics (AIMD) calculations. These simulations were performed at 10 K and 300 K, shown in Figure S2 in the Supporting Information, demonstrating that these GBs remain stable under low and room temperatures.

Figure 4(a) demonstrates a common type of mirror-image GB where two inverse domains are connected through sulfur atoms. This structure has a band crossing the Fermi level, contributed by the hybridization of $d_{x^2-y^2}$ orbitals of molybdenum atoms and p_x orbitals of sulfur atoms as previously predicted.[19] However, displacements of both molybdenum and sulfur atoms are observed after full relaxation, as shown in Figure 4(a). These displacements cause trimerization, extending the lattice constant from a to $3a$. Such small displacements

lead to significant changes in the electronic properties. The previously continuous electron wavefunction becomes localized, demonstrating a transition from metallic to semiconducting states. This transition is further evidenced by the band structure of the trimerized GB, as shown in Figure 4(a), where an energy gap of 0.9 eV is clearly present. Spontaneous trimerization can sometimes lead to unit cell reconstruction, as shown in the second example of a mirror-image GB in Figure 4(b). Upon relaxation, a profound transformation occurs in the unit cell structure, causing a transition from metallic to semiconducting states, with localized states and a gap of 0.4 eV observed in the band structure. The third GB shows the transition due to the introduction of periodic defects. Figure 4(c) shows the 4|8 GB, achieved by introducing a periodic vacancy defect in one of the sulfur atoms along the 4|4P GB. Such GBs have been observed experimentally.[14] These vacancy defects also triple the lattice periodicity to $3a$. With these vacancies, a band gap of approximately 0.1 eV is observed, and the previously conducting wavefunction shows discontinuous behavior.

Metallic grain boundaries

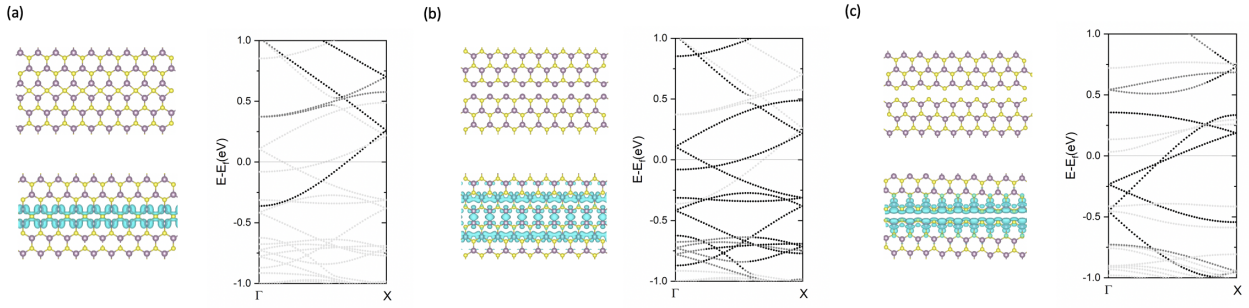

Figure 5: Stable metallic mirror-imaged grain boundaries of (a) 4|4P grain boundaries, (b) Mo-Mo bridging grain boundaries, and (c) S-S bridging grain boundaries. For each type, the fully relaxed structure, square of the electron wavefunction, and band structure are shown in order. The isosurface level of the electron density plot is 0.258 e/Å^3.

The preceding examples illustrate various mechanisms through which MoS_2 GBs undergo a MS transition. Conversely, some GBs can retain their metallic properties as the energetically favorable state, primarily due to strong elastic bonding from the supports, as suggested by our theoretical model.

A prominent example of a metallic GB is the well-studied 4|4P configuration,[29,54] shown in Figure 5(a). In this configuration, the zigzag edges are aligned by merging the sulfur atoms situated between them. Upon full relaxation, the structure exhibits minimal change, retaining its original periodicity. Our calculations confirm that this type of GB maintains its metallic nature, as evidenced by a dispersion line crossing the Fermi level. The wave function analysis at the crossing point reveals two distinct conducting paths primarily along the Mo atoms near the GB. Detailed analysis indicates that these conducting paths originate from d_{yz} orbitals of the Mo atoms, consistent with prior theoretical predictions.[8,19] Furthermore, our investigation demonstrates that including spin degrees of freedom or introducing on-site Coulomb interactions does not alter the conducting properties of these metallic GBs.

In addition to the well-recognized 4|4P GB, we have identified two new GBs that exhibit thermodynamic stability and metallic properties. One such GB, illustrated in Figure 5(b), features direct alignment of the zigzag edges of Mo atoms. We refer to it as the Mo-Mo bridging GB. After full relaxation, the Mo-Mo bridging GB undergoes an overall atomic shift. However, its periodicity is preserved as a, displaying bands crossing the Fermi level. Interestingly, the primary conducting path at this GB does not follow the Mo atom closest to the boundary. Instead, it predominantly occurs along the Mo atom located at a distance from the GB, primarily attributed to d_{xy}, d_{z^2}, and $d_{x^2-y^2}$ orbitals of Mo atoms.

We have also observed metallic behavior in S-S bridging GBs shown in Figure 5(c). Despite the relaxation-induced shifts in sulfur atom positions, the lattice constant maintains as a. Our calculations confirm that this type of GB retains its metallic nature, as evidenced by metallic bands crossing the Fermi level in the band structure shown. Furthermore, the wave function analysis at the Fermi level reveals conducting paths along the S-S bridging GB, involving d_{z^2} and $d_{x^2-y^2}$ orbitals of Mo atoms and p_x orbitals of the sulfur atoms.

A common property among these three GBs is that any horizontal displacement of the GB atoms results in a change in the length of the Mo-S bond. For example, any displacement in the x-direction of the sulfur atom in the 4|4P and S-S bridging GBs, as well as Mo atoms

in the Mo-Mo bridging GBs, will alter the Mo-S bond length. However, this phenomenon is not observed in all semiconducting structures, where displacements can occur through bond rotation without affecting bond length. This implies that atoms in these three GBs experience stronger bond stiffness and larger elastic forces from supports. These examples of metallic phases of mirror-image GBs further support our theoretical model that, if electron transfer is permitted, the 1D structure will maintain stable metallic phases if it receives strong support from the 2D lattice.

Conclusion

In conclusion, we have explored the stability of metallic one-dimensional structure supported by hexagonal 2D lattices. Using open system tight-binding model, we show that thought spontaneous trimerization and metal-to-semiconductor transition may occurs for unsupported 1D chain, the elastic support from 2D lattice can suppress this and stabilize the metallic phase if electron transfer is permitted. Using first-principles calculations, we further verified this theory by showing that GBs that will undergo metal-to-semiconductor transition if the GB atoms are weakly bonded, and remain metallic otherwise. Through this theory, we predict two new GBs with strongly bonded GB atoms that are stable in the metallic phase. These results emphasize the crucial role of lattice support in maintaining the metallic state and provide insights for designing stable 1D metallic systems for nanoelectronic and quantum applications.

Acknowledgement

This work was supported by the National Research Foundation, Singapore under Award No. NRF-CRP24-2020-0002. Y.-W.Z. acknowledges the support from Singapore A*STAR SERC CRF Award. The use of computing resources at the A*STAR Computational Centre and National Supercomputer Centre, Singapore is gratefully acknowledged.

Notes

The authors declare no conflict of interest.

References

(1) Peierls, R. Zur kinetischen Theorie der Wärmeleitung in Kristallen. *Annalen der Physik* **1929**, *395*, 1055–1101.

(2) Walatka, V. V.; Labes, M. M.; Perlstein, J. H. Polysulfur Nitride—a One-Dimensional Chain with a Metallic Ground State. *Phys. Rev. Lett.* **1973**, *31*, 1139–1142.

(3) Krieger, Y. H. Structural instability of one-dimensional systems as a physical principle underlying the functioning of molecular electronic devices. *Journal of Structural Chemistry* **1999**, *40*, 594–619.

(4) Snijders, P. C.; Weitering, H. H. Colloquium: Electronic instabilities in self-assembled atom wires. *Rev. Mod. Phys.* **2010**, *82*, 307–329.

(5) Zhao, J. Z.; Fan, W.; Verstraete, M. J.; Zanolli, Z.; Fan, J.; Yang, X. B.; Xu, H.; Tong, S. Y. Quasi-One-Dimensional Metal-Insulator Transitions in Compound Semiconductor Surfaces. *Phys. Rev. Lett.* **2016**, *117*, 116101.

(6) Liu, Y.-W.; Zhan, Z.; Wu, Z.; Yan, C.; Yuan, S.; He, L. Realizing One-Dimensional Electronic States in Graphene via Coupled Zeroth Pseudo-Landau Levels. *Phys. Rev. Lett.* **2022**, *129*, 056803.

(7) Davies, F. H.; Krasheninnikov, A. V. Chains of atoms embedded into transition metal dichalcogenides as one-dimensional half-metallic magnets. *Phys. Rev. B* **2024**, *109*, 165442.

(8) Zhang, S.; Huang, B.; Dai, Y.; Wei, W. One-Dimensional Metallic Grain Boundary in Transition Metal Dichalcogenides. *Computational Materials Science* **2022**, *203*, 111115.

(9) Little, W. A. Possibility of Synthesizing an Organic Superconductor. *Phys. Rev.* **1964**, *134*, A1416–A1424.

(10) Grigorenko, A.; Bending, S.; Tamegai, T.; Ooi, S.; Henini, M. A one-dimensional chain state of vortex matter. *Nature* **2001**, *414*, 728–731, Publisher: Nature Publishing Group.

(11) Kim, H. W. Recent Progress in the Role of Grain Boundaries in Two-Dimensional Transition Metal Dichalcogenides Studied Using Scanning Tunneling Microscopy/Spectroscopy. *Applied Microscopy* **2023**, *53*, 5.

(12) Su, W. P.; Schrieffer, J. R.; Heeger, A. J. Solitons in Polyacetylene. *Physical Review Letters* **1979**, *42*, 1698–1701.

(13) Su, W. P.; Schrieffer, J. R.; Heeger, A. J. Soliton Excitations in Polyacetylene. *Physical Review B* **1980**, *22*, 2099–2111.

(14) Van Der Zande, A. M.; Huang, P. Y.; Chenet, D. A.; Berkelbach, T. C.; You, Y.; Lee, G.-H.; Heinz, T. F.; Reichman, D. R.; Muller, D. A.; Hone, J. C. Grains and Grain Boundaries in Highly Crystalline Monolayer Molybdenum Disulphide. *Nature Materials* **2013**, *12*, 554–561.

(15) Bristowe, N. C.; Stengel, M.; Littlewood, P. B.; Artacho, E.; Pruneda, J. M. One-Dimensional Half-Metallic Interfaces of Two-Dimensional Honeycomb Insulators. *Physical Review B* **2013**, *88*, 161411.

(16) Liu, H.; Jiao, L.; Yang, F.; Cai, Y.; Wu, X.; Ho, W.; Gao, C.; Jia, J.; Wang, N.; Fan, H.; et al. Dense Network of One-Dimensional Midgap Metallic Modes in Monolayer MoSe 2 and Their Spatial Undulations.

(17) Ly, T. H.; Perello, D. J.; Zhao, J.; Deng, Q.; Kim, H.; Han, G. H.; Chae, S. H.;

Jeong, H. Y.; Lee, Y. H. Misorientation-Angle-Dependent Electrical Transport across Molybdenum Disulfide Grain Boundaries. *Nature Communications* **2016**, *7*, 10426.

(18) Ma, Y.; Diaz, H. C.; Avila, J.; Chen, C.; Kalappattil, V.; Das, R.; Phan, M.-H.; Čadež, T.; Carmelo, J. M. P.; Asensio, M. C.; et al. Angle Resolved Photoemission Spectroscopy Reveals Spin Charge Separation in Metallic MoSe2 Grain Boundary.

(19) Gibertini, M.; Marzari, N. Emergence of One-Dimensional Wires of Free Carriers in Transition-Metal-Dichalcogenide Nanostructures. *Nano Letters* **2015**, *15*, 6229–6238.

(20) Krishnamurthi, S.; Brocks, G. 1D Metallic States at 2D Transition Metal Dichalcogenide Semiconductor Heterojunctions. *npj 2D Materials and Applications* **2021**, *5*, 1–6.

(21) Lin, J.; Pantelides, S. T.; Zhou, W. Vacancy-Induced Formation and Growth of Inversion Domains in Transition-Metal Dichalcogenide Monolayer. *ACS Nano* **2015**, *9*, 5189–5197.

(22) Ma, Y.; Kolekar, S.; Coy Diaz, H.; Aprojanz, J.; Miccoli, I.; Tegenkamp, C.; Batzill, M. Metallic Twin Grain Boundaries Embedded in MoSe $_2$ Monolayers Grown by Molecular Beam Epitaxy. *ACS Nano* **2017**, *11*, 5130–5139.

(23) Najmaei, S.; Liu, Z.; Zhou, W.; Zou, X.; Shi, G.; Lei, S.; Yakobson, B. I.; Idrobo, J.-C.; Ajayan, P. M.; Lou, J. Vapour Phase Growth and Grain Boundary Structure of Molybdenum Disulphide Atomic Layers. *Nature Materials* **2013**, *12*, 754–759.

(24) Zhou, W.; Zou, X.; Najmaei, S.; Liu, Z.; Shi, Y.; Kong, J.; Lou, J.; Ajayan, P. M.; Yakobson, B. I.; Idrobo, J.-C. Intrinsic Structural Defects in Monolayer Molybdenum Disulfide. *Nano Letters* **2013**, *13*, 2615–2622.

(25) Le, D.; Rahman, T. S. Joined Edges in MoS $_2$: Metallic and Half-Metallic Wires. *Journal of Physics: Condensed Matter* **2013**, *25*, 312201.

(26) Park, J.; Xue, K.-H.; Mouis, M.; Triozon, F.; Cresti, A. Electron Transport Properties of Mirror Twin Grain Boundaries in Molybdenum Disulfide: Impact of Disorder. *Physical Review B* **2019**, *100*, 235403.

(27) Chowdhury, S.; Rigosi, A. F.; Hill, H. M.; Vora, P.; Hight Walker, A. R.; Tavazza, F. Computational Methods for Charge Density Waves in 2D Materials. *Nanomaterials* **2022**, *12*, 504.

(28) Kan, M.; Wang, J. Y.; Li, X. W.; Zhang, S. H.; Li, Y. W.; Kawazoe, Y.; Sun, Q.; Jena, P. Structures and Phase Transition of a MoS $_2$ Monolayer. *The Journal of Physical Chemistry C* **2014**, *118*, 1515–1522.

(29) Barja, S.; Wickenburg, S.; Liu, Z.-F.; Zhang, Y.; Ryu, H.; Ugeda, M. M.; Hussain, Z.; Shen, Z.-X.; Mo, S.-K.; Wong, E.; et al. Charge Density Wave Order in 1D Mirror Twin Boundaries of Single-Layer MoSe2. *Nature Physics* **2016**, *12*, 751–756.

(30) Bin Subhan, M. K.; Suleman, A.; Moore, G.; Phu, P.; Hoesch, M.; Kurebayashi, H.; Howard, C. A.; Schofield, S. R. Charge Density Waves in Electron-Doped Molybdenum Disulfide. *Nano Letters* **2021**, *21*, 5516–5521.

(31) Choi, J.-H.; Liu, S.; Zhang, W.; Liu, Z.; Rummeli, M. H. Charge Density Waves Driven by Peierls Instability at the Interface of Two-Dimensional Lateral Heterostructures. *Small* **2018**, *14*, 1803040.

(32) Krishnamurthi, S.; Brocks, G. Spin/Charge Density Waves at the Boundaries of Transition Metal Dichalcogenides. *Physical Review B* **2020**, *102*, 161106.

(33) Jadaun, P.; Xiao, D.; Niu, Q.; Banerjee, S. K. Topological Classification of Crystalline Insulators with Space Group Symmetry. *Physical Review B* **2013**, *88*, 085110.

(34) Liu, F.-H.; Fu, W.; Deng, Y.-H.; Yuan, Z.-B.; Wu, L.-N. First-principles study of the Kohn anomaly in TaTe4. *Applied Physics Letters* **2021**, *119*, 091901.

(35) Randle, M. D.; Lipatov, A.; Mansaray, I.; Han, J. E.; Sinitskii, A.; Bird, J. P. Collective states and charge density waves in the group IV transition metal trichalcogenides. *Applied Physics Letters* **2021**, *118*, 210502.

(36) Martinez Alvarez, V. M.; Coutinho-Filho, M. D. Edge states in trimer lattices. *Phys. Rev. A* **2019**, *99*, 013833.

(37) Baeriswyl, D.; Maki, K. Electron Correlations in Polyacetylene. *Physical Review B* **1985**, *31*, 6633–6642.

(38) Kivelson, S.; Heim, D. E. Hubbard versus Peierls and the Su-Schrieffer-Heeger Model of Polyacetylene. *Physical Review B* **1982**, *26*, 4278–4292.

(39) Hirsch, J. E. Effect of Coulomb Interactions on the Peierls Instability. *Physical Review Letters* **1983**, *51*, 296–299.

(40) Dzierzawa, M.; Mocanu, C. The Peierls–Hubbard Model at Weak Coupling. *Journal of Physics: Condensed Matter* **2005**, *17*, 2663.

(41) Sengupta, P.; Sandvik, A. W.; Campbell, D. K. Peierls Transition in the Presence of Finite-Frequency Phonons in the One-Dimensional Extended Peierls-Hubbard Model at Half-Filling. *Physical Review B* **2003**, *67*, 245103.

(42) Cai, X.; Li, Z.-X.; Yao, H. Antiferromagnetism Induced by Bond Su-Schrieffer-Heeger Electron-Phonon Coupling: A Quantum Monte Carlo Study. *Physical Review Letters* **2021**, *127*, 247203.

(43) Clay, R. T.; Hardikar, R. P. Intermediate Phase of the One Dimensional Half-Filled Hubbard-Holstein Model. *Physical Review Letters* **2005**, *95*, 096401.

(44) Weiss, U. *Quantum Dissipative Systems*; WORLD SCIENTIFIC, 1993.

(45) Breuer, H.; Petruccione, F. *The Theory of Open Quantum Systems*; Oxford University Press, 2002.

(46) Lindblad, G. On the generators of quantum dynamical semigroups. *Communications in Mathematical Physics* **1976**, *48*, 119–130.

(47) Gorini, V.; Kossakowski, A.; Sudarshan, E. C. G. Completely positive dynamical semigroups of N-level systems. *Journal of Mathematical Physics* **1976**, *17*, 821–825.

(48) Kresse, G.; Furthmüller, J. Efficient Iterative Schemes for Ab Initio Total-Energy Calculations Using a Plane-Wave Basis Set. *Physical Review B* **1996**, *54*, 11169–11186.

(49) Kresse, G.; Joubert, D. From Ultrasoft Pseudopotentials to the Projector Augmented-Wave Method. *Physical Review B* **1999**, *59*, 1758–1775.

(50) Gao, N.; Guo, Y.; Zhou, S.; Bai, Y.; Zhao, J. Structures and Magnetic Properties of MoS_2 Grain Boundaries with Antisite Defects. *The Journal of Physical Chemistry C* **2017**, *121*, 12261–12269.

(51) Qiu, X.; Wang, Y.; Jiang, Y. Dopants and Grain Boundary Effects in Monolayer MoS_2 : A First-Principles Study. *Physical Chemistry Chemical Physics* **2021**, *23*, 11937–11943.

(52) Yu, Z. G.; Zhang, Y.-W.; Yakobson, B. I. An Anomalous Formation Pathway for Dislocation-Sulfur Vacancy Complexes in Polycrystalline Monolayer MoS_2. *Nano Letters* **2015**, *15*, 6855–6861.

(53) Hong, J. et al. Exploring Atomic Defects in Molybdenum Disulphide Monolayers. *Nature Communications* **2015**, *6*, 6293.

(54) Zou, X.; Liu, Y.; Yakobson, B. I. Predicting Dislocations and Grain Boundaries in Two-Dimensional Metal-Disulfides from the First Principles. *Nano Letters* **2013**, *13*, 253–258.